Vol 446|15 March 2007|doi:10.1038/nature05615

LETTERS

Evolution and diversity of subduction zones controlled by slab width

W. P. Schellart[1], J. Freeman[1], D. R. Stegman[2], L. Moresi[2] & D. May[2]

Subducting slabs provide the main driving force for plate motion and flow in the Earth's mantle[1–4], and geodynamic, seismic and geochemical studies offer insight into slab dynamics and subduction-induced flow[3–15]. Most previous geodynamic studies treat subduction zones as either infinite in trench-parallel extent[3,5,6] (that is, two-dimensional) or finite in width but fixed in space[7,16]. Subduction zones and their associated slabs are, however, limited in lateral extent (250–7,400 km) and their three-dimensional geometry evolves over time. Here we show that slab width controls two first-order features of plate tectonics—the curvature of subduction zones and their tendency to retreat backwards with time. Using three-dimensional numerical simulations of free subduction, we show that trench migration rate is inversely related to slab width and depends on proximity to a lateral slab edge. These results are consistent with retreat velocities observed globally, with maximum velocities (6–16 cm yr^{-1}) only observed close to slab edges (<1,200 km), whereas far from edges (>2,000 km) retreat velocities are always slow (<2.0 cm yr^{-1}). Models with narrow slabs (≤1,500 km) retreat fast and develop a curved geometry, concave towards the mantle wedge side. Models with slabs intermediate in width (~2,000–3,000 km) are sublinear and retreat more slowly. Models with wide slabs (≥4,000 km) are nearly stationary in the centre and develop a convex geometry, whereas trench retreat increases towards concave-shaped edges. Additionally, we identify periods (5–10 Myr) of slow trench advance at the centre of wide slabs. Such wide-slab behaviour may explain mountain building in the central Andes, as being a consequence of its tectonic setting, far from slab edges.

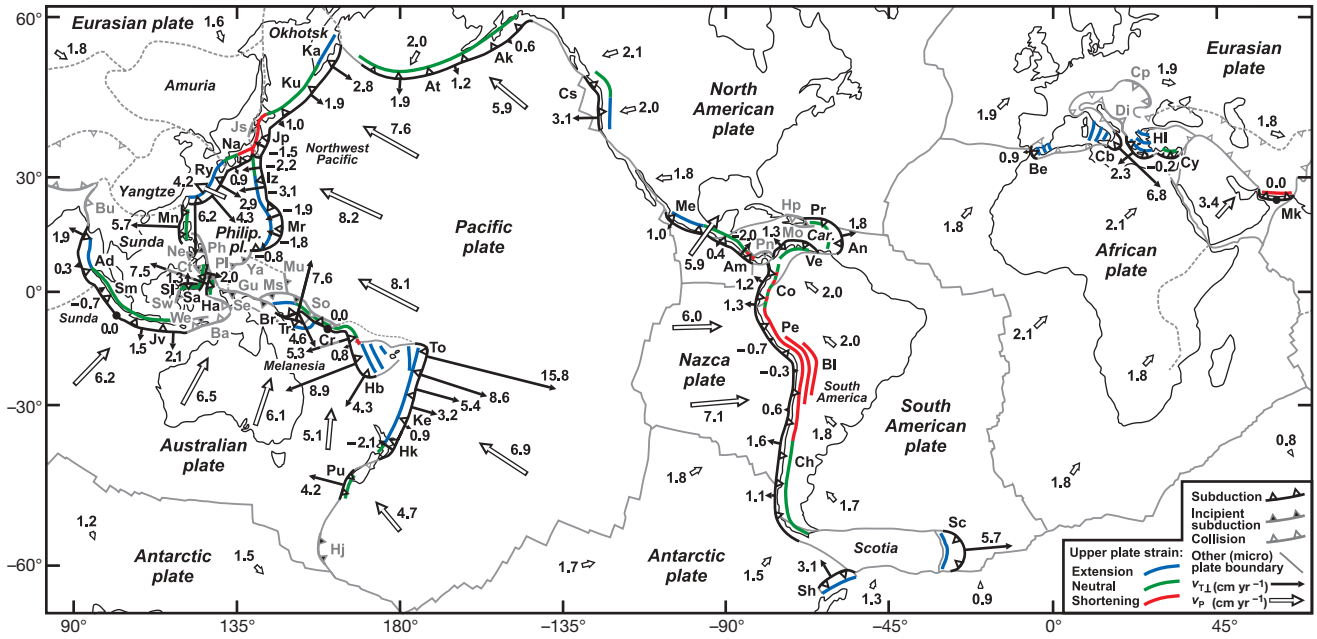

Figure 1 | The major subduction zones on Earth for which the trench-perpendicular trench migration velocity ($v_{T\perp}$) has been calculated. Black arrows illustrate $v_{T\perp}$ vectors, while open arrows illustrate plate velocity (v_P) vectors for 11 major plates. Velocities were calculated using the relative plate motion model from ref. 27 in the Indo-Atlantic hotspot reference frame[28]. Subduction zones: Ad, Andaman; Ak, Alaska; Am, Central America; An, Lesser Antilles; At, Aleutian; Be, Betic Rif; Bl, Bolivia; Br, New Britain; Cb, Calabria; Ch, Chile; Co, Colombia; Cr, San Cristobal; Cs, Cascadia; Cy, Cyprus; Ha, Halmahera; Hb, New Hebrides; Hk, Hikurangi; Hl, Hellenic; Iz, Izu-Bonin; Jp, Japan; Jv, Java; Ka, Kamchatka; Ke, Kermadec; Ku, Kuril; Me, Mexico; Mk, Makran; Mn, Manila; Mr, Mariana; Na, Nankai; Pe, Peru; Pr, Puerto Rico; Pu, Puysegur; Ry, Ryukyu; Sa, Sangihe; Sc, Scotia; Sh, South Shetland; Sl, North Sulawesi; Sm, Sumatra; To, Tonga; Tr, Trobriand; Ve, Venezuela. Collision zones: Ba, Banda; Bu, Burma; Cp, Carpathian; Di, Dinaride; Hp, Hispaniola; Se, Seram; So, Solomon. Incipient subduction zones: Ct, Cotobato; Gu, New Guinea; Hj, Hjort; Js, Japan Sea; Mo, Muertos; Ms, Manus; Mu, Mussau; Ne, Negros; Ph, Philippine; Pl, Palau; Pn, Panama; Sw, West Sulawesi; We, Wetar; Ya, Yap. Incipient subduction zones are young (≤5 Myr), have a short slab (≤150 km) and, together with collision zones, have been excluded from the trench migration calculations in Fig. 2. Trench migration rates for incipient subduction zones are presented in Supplementary Fig. 1.

[1]Research School of Earth Sciences, The Australian National University, Canberra, Australian Capital Territory 0200, Australia. [2]School of Mathematical Sciences, Monash University, Melbourne, Victoria 3800, Australia.

Seismological and geochemical studies suggest that mantle material flows around lateral slab edges towards the mantle wedge[10,12–15]. Such flow is explained as return flow induced by retreat of the trench and rollback of the slab[17,18]. It is expected that lateral slab edges promote rapid rollback by facilitating return flow around the edges instead of underneath the slab tip, as imposed by two-dimensional geometry[17,19]. In nature, the fastest trench-perpendicular trench migration velocities ($v_{T\perp}$ = 6–16 cm yr^{-1}) are indeed observed within 1,200 km of slab edges, whereas at distances >2,000 km $v_{T\perp}$ is <2.0 cm yr^{-1} (Figs 1, 2). Rapid retreat velocities are comparable to fast plate velocities. Figure 2 indicates that proximity to a slab edge is required for, but does not guarantee, rapid trench retreat. Such complexity is expected, because retreat velocity also depends on other factors, including slab density, thickness and length[17], and the rate of tearing between slab and plate at the slab edge, which depends on plate strength[16,20]. These factors generally differ between subduction zones.

Our calculations imply that trench migration is of global importance. For the ~48,800 km of trench considered, 27.6% of the total subduction rate is due to trench migration (mean $v_{T\perp}$ of 1.51 cm yr^{-1} from a total mean convergence of 5.47 cm yr^{-1}). Furthermore, trench migration induces a global upper-mantle volume flux of ~539 km^3 yr^{-1} around the laterally migrating slabs (assuming that $v_{T\perp}$ is constant with depth). This flux expresses itself primarily as toroidal flow[17,21], inducing significant mantle stirring. For comparison, the poloidal mantle flux resulting from trenchward subducting plate motion is only ~193 km^3 yr^{-1} (assuming a constant plate thickness of 100 km).

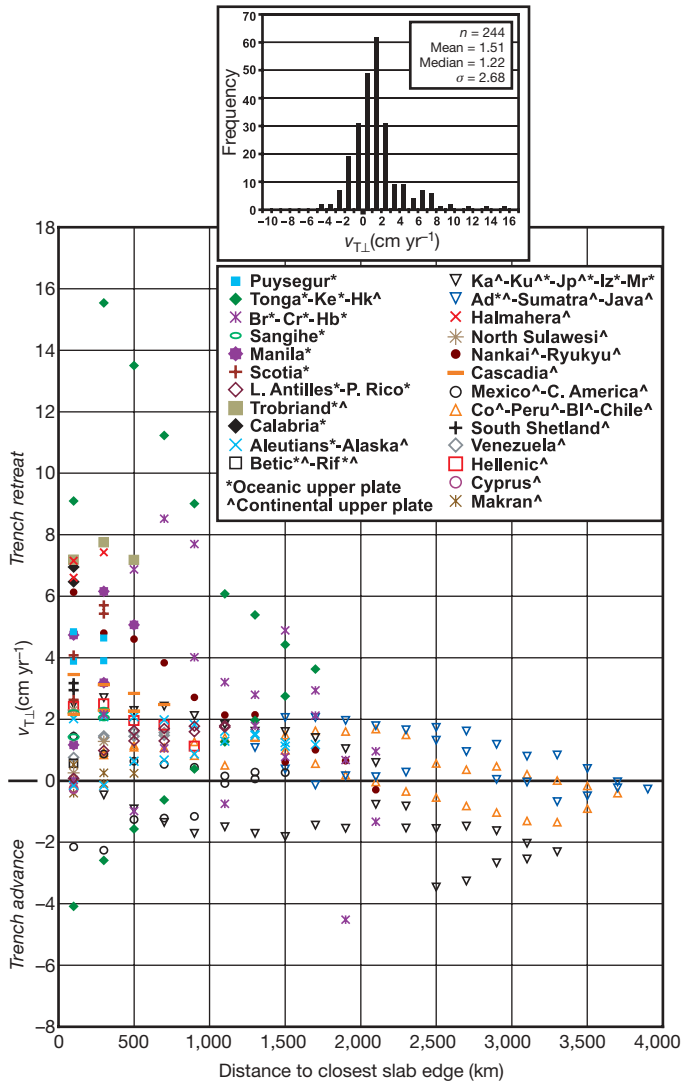

Figure 2 | The proximity of subduction zone segments (200 km wide in trench-parallel extent) to the closest lateral slab edge, plotted against $v_{T\perp}$ for all subduction zones on Earth. Velocities were calculated using the relative plate motion model from ref. 27 in the Indo-Atlantic hotspot reference frame[28]. Positive velocities indicate trench retreat. For details on trench migration calculations see Supplementary Information. Abbreviations as Fig. 1. Inset shows a frequency plot of trench migration velocities for the 244 trench segments investigated.

Recent studies have focused on three-dimensional aspects of subduction zones[17,18,21], but only investigated slab widths ≤1,500 km. We conduct three-dimensional numerical experiments, which for the first time explore the entire range of slab widths (W) found in nature (300–7,000 km). Our experiments are performed with the program 'Underworld' and share the same model design as those of ref. 21, but introduce the important modification of a two-layered plate (a viscoplastic upper half and a viscous lower half). This limits the strength of the upper half, simulating weakening in the brittle upper lithosphere, and allows significant slab–plate coupling through the viscous bottom half to drive plate motion. The subducting plate is laterally homogeneous, thus ignoring trench-parallel buoyancy variation due to aseismic ridges/plateaus and change in lithospheric age, which affect trench geometry and velocity[17,21,22]. Boundary effects have been minimized by implementing widely spaced free-slip boundaries (see Supplementary Information).

Figure 3 shows a wide-slab model (W = 6,000 km) that is representative of simulations with W = 4,000–7,000 km. Initially, trenchward plate motion and trench retreat are slow while the slab dip increases progressively. Trench retreat is accompanied by slab rollback, inducing upper-mantle return flow around the lateral slab edges. Plate and trench velocity increase with time owing to increase in slab length until the slab tip approaches the transition zone. In the centre, trench retreat decelerates and changes to trench advance, while the slab is folded on top of the discontinuity with large recumbent folds (Supplementary Movie 1). Trenchward plate motion remains relatively fast at several cm yr^{-1}. Trench migration in the centre becomes episodic, with phases of retreat and advance ($-1.5 < v_{T\perp} < 1.0$ cm yr^{-1}). Near the slab edges, the trench is predominantly retreating (up to 6.0 cm yr^{-1}, Supplementary Fig. 2), producing a slab-draping geometry on the transition zone.

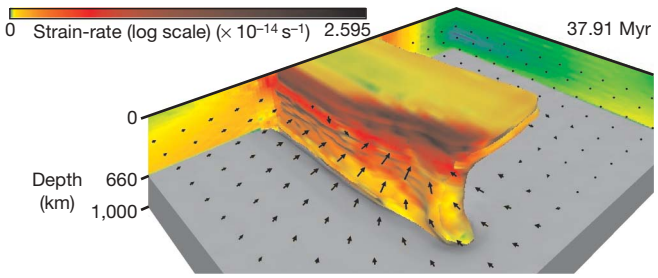

Figure 3 | Image illustrating a wide-slab subduction experiment. (Here W = 6,000 km; see also Supplementary movie 1.) Note that only half of the model is shown (and calculated), because the experiment is symmetrical with respect to a plane through the centre of the subduction zone. Subduction is driven by buoyancy forces only, reflecting natural subduction systems. A 100-km-thick high-viscosity plate (oceanic lithosphere) overlies 900 km of lower-density mantle, subdivided into 560 km of low-viscosity upper mantle and 340 km of high-viscosity lower mantle, confined in a three-dimensional cartesian box. Each experiment started with a 187-km-long slab dipping at 15.5°. Details on the numerical method can be found in Supplementary Information and in ref. 21. The models exclude an overriding plate and elasticity, thereby overestimating slab dip angles[21]. The plate has a viscoplastic upper half and a viscous lower half. The viscosity of the lower half was set to be 200 times the upper-mantle viscosity, producing plate-like behaviour and significant slab–plate coupling to drive plate motion as observed in laboratory simulations[4,17]. Black vectors are located at 200 km depth and illustrate the horizontal flow pattern in the mantle.

Intermediate-width slabs ($W = 2{,}000$–$3{,}000$ km) predominantly retreat at intermediate velocities and produce recumbent folds and minor draping at the transition zone (Supplementary Movie 2). Narrow slabs (300–1,500 km) show the fastest trench retreat velocities but the slowest plate velocities, resulting in slab draping on top of the transition zone (Supplementary Movie 3).

The numerical results show an inverse dependence of $v_{T\perp}$ on W: the wider the slab, the smaller the retreat velocity (Fig. 4a). All models show a local maximum for $v_{T\perp}$ for a slab penetration depth of 400–500 km, that is, before slab tip–transition zone interaction, followed by a decrease in $v_{T\perp}$. For $W \leq 1{,}500$ km, trench retreat dominates ($-0.4 \leq v_{T\perp} \leq 10.0$ cm yr^{-1}), whereas for $W \geq 2{,}000$ km, periods of notable trench advance occur. W also influences $v_{T\perp}$ along the trench itself. For $W \leq 1{,}500$ km, $v_{T\perp}$ is maximum in the centre and decreases towards the edges, thereby forming a curved trench that is concave towards the mantle wedge side (Fig. 4b). For $W \approx 2{,}000$–$3{,}000$ km, $v_{T\perp}$ is of comparable magnitude along the trench, resulting in a more rectilinear trench (Fig. 4c). For $W \geq \sim 4{,}000$ km, $v_{T\perp}$ is minimum in the centre and maximum close to each slab edge (Fig. 4a and d, Supplementary Fig. 2). This results in an overall convex-shaped trench with concave-shaped edges while the slab folds itself around an upper-mantle 'stagnation zone', which experiences minor volume exchange with the mantle wedge. Here, circulation is comparable to two-dimensional models with two poloidal flow cells separated by the slab.

The inverse dependence between W and $v_{T\perp}$ is unexpected, as the face-wise sinking velocity of an oblate ellipsoid through an infinite volume fluid at low Reynolds number ($\ll 1$) depends on the shape of the ellipsoid and the square of the effective diameter[23].

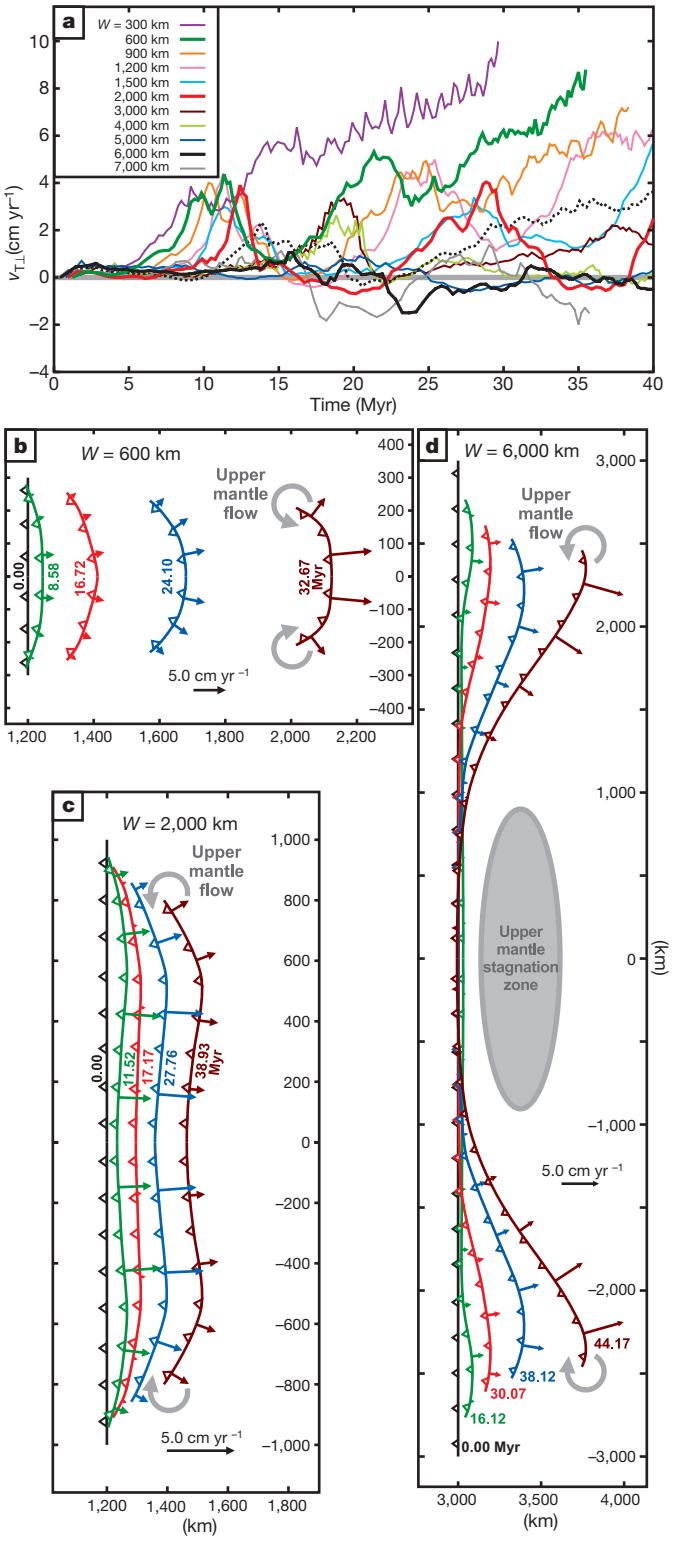

Figure 4 | Influence of W on $v_{T\perp}$ and subduction zone geometry. **a**, Diagram illustrating the influence of W on $v_{T\perp}$ (measured in the centre of the subduction zone; solid lines). For $W = 6{,}000$ km, trench migration velocity (v_T) at 758 km from the slab edge is also plotted (black dotted line). **b**–**d**, Diagrams showing the progressive evolution of the subduction zone for three simulations with a different W. **b**, $W = 600$ km; **c**, $W = 2{,}000$ km; **d**, $W = 6{,}000$ km. Time is given in million years (Myr). Note different length scale in **b**–**d**.

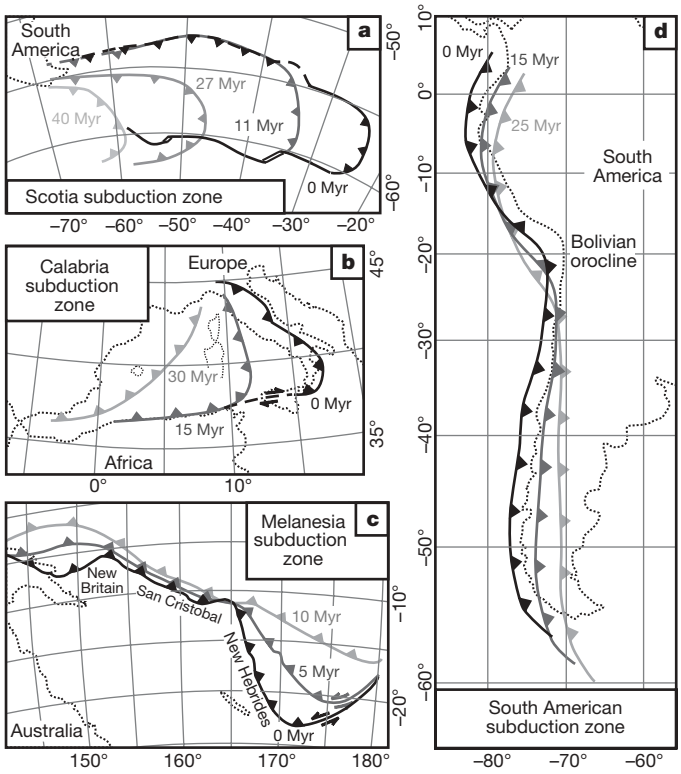

Figure 5 | Progressive evolution of four subduction zones with a different W (measured at the earliest time of the reconstruction). **a**, Evolution of the Scotia subduction zone, $W = 800$ km (modified from ref. 29); **b**, Evolution of the Calabrian subduction zone[11], $W = 1{,}200$ km; **c**, Evolution of the Melanesian subduction zone[20], $W = 4{,}400$ km; **d**, Evolution of the South American subduction zone, $W = 7{,}000$ km, with South American plate motion from ref. 30, adopting a Miocene–Present shortening model for the Andes with a maximum shortening of 350 km in the Bolivian orocline[24] and incorporating accretion/erosion along the trench (see Supplementary Information). Subduction zone migration has been plotted in the following reference frames: **a**, South American plate; **b**, Eurasian plate; **c**, Australian plate; **d**, Indo-Atlantic hotspots. Numerals with Myr indicate time in Myr before the present.

That relationship predicts that the sinking velocity for the widest slab (7,000 km) is 6–25 times faster than for the narrowest slab (300 km), the exact ratio depending on slab length, which suggests that $v_{T\perp}$ increases with increasing slab width. However, the opposite is observed in both nature and experiments. The experiments illustrate that this can be ascribed to the finite upper-mantle thickness that is small compared to W, and complicated rollback-induced flow patterns that are oriented (almost) exclusively around the lateral slab edges (95–100% of the mantle flux)[17,21]. Rollback-induced flow in the upper mantle exerts a viscous drag at the upper–lower mantle boundary that roughly increases with the square of W, while the total slab buoyancy force, which drives sinking and slab retreat, only increases linearly with W. Other complicating factors include slab deformability, allowing variation of $v_{T\perp}$ along the trench.

The models show that rollback-induced return flow produces concave trenches within ~800 km of slab edges, in agreement with the geometry of retreating trench segments near slab edges (Fig. 1). The models further show that subduction zones 300–1,500 km wide become concave, comparable to natural examples with $W < 1{,}600$ km (13 out of 14 are concave), those 2,000–3,000 km wide remain sublinear, comparable to natural examples with $W = 1{,}700$–$3{,}550$ km (4 out of 6 are sublinear), and those 4,000–7,000 km wide become convex, comparable to natural examples with $W = 4{,}400$–$7{,}850$ km (3 out of 4 are convex) (see Supplementary Table 1). The models further agree with the long-term trench kinematics of narrow (Scotia and Calabria, Fig. 5a, b) and wide (Fig. 5c, d) subduction zones, and explain why the four widest subduction zones on Earth (South America, Sunda, Northwest Pacific and Melanesia) are nearly stationary or advancing in the centre.

The Melanesia subduction zone evolved into an overall convex geometry with concave-shaped edges (Fig. 5c). The central San Cristobal segment is nearly stationary with a neutral overriding plate, while the New Britain and New Hebrides segments are retreating, inducing backarc spreading (Manus and North Fiji basins)[20]. The convex Northwest Pacific subduction zone undergoes shortening and trench advance in the centre (Japan), which can be explained by the modelling. Both edges are concave and experience backarc opening (Mariana trough, Central Kamchatka graben) (Fig. 1). Trench advance along the Izu-Bonin-Mariana segment is partly explained by the modelling and partly by rapid westward motion of the overriding Philippine plate and subduction of the Ogasawara plateau and the Caroline ridge. The Sunda subduction zone is not convex, but is nearly stationary in the centre (Sumatra section) and retreating near the northwestern edge (Andaman section with active backarc spreading) and eastern edge (Java section) (Fig. 1). The easternmost Banda section experienced Neogene trench retreat and backarc opening of the Banda Sea before arc–continent collision.

Formation of the Andes mountains and the Bolivian orocline has remained an enigma, as they formed at a subduction zone and not at a continental collision zone such as the Himalayas. A reconstruction of the South American subduction zone shows that it developed a convex geometry with concave edges, whereas the Bolivian orocline has remained nearly stationary for the past 25 Myr (Fig. 5d). The orocline is characterized by compression, orogenesis and shortening in the overriding plate, decreasing progressively northward and southward[24]. Shear wave splitting in the mantle under the South American slab suggests trench-parallel flow in the north and south but negligible trench-parallel flow beneath the orocline[10]. This is consistent with the mantle stagnation zone observed below convex-shaped centres of wide slabs (Fig. 4d). The stagnation zone is capable of supporting large compressive stresses at the subduction interface induced by trenchward overriding plate motion. Indeed, the South American plate is driven westward (Fig. 1) by a combination of forces: suction from the Nazca slab[1,3], slab pull from the Scotia and Lesser Antilles slabs[4,25], and ridge push from the Mid-Atlantic Ridge[25]. Stagnation zone development and intermittent trench advance at the centre of wide slabs can therefore explain enigmatic features of the Central Andes, including mountain building above a subduction zone, the presence of a geoid high below the Bolivian orocline[10] and a rapid increase in palaeo-elevation[26].

Received 8 June 2006; accepted 18 January 2007.

1. Elsasser, W. M. Sea-floor spreading as thermal convection. *J. Geophys. Res.* **76,** 1101–1112 (1971).
2. Forsyth, D. W. & Uyeda, S. On the relative importance of the driving forces of plate motion. *Geophys. J. R. Astron. Soc.* **43,** 163–200 (1975).
3. Zhong, S. & Gurnis, M. Mantle convection with plates and mobile, faulted plate margins. *Science* **267,** 838–843 (1995).
4. Schellart, W. P. Quantifying the net slab pull force as a driving mechanism for plate tectonics. *Geophys. Res. Lett.* **31,** L07611, doi:10.1029/2004GL019528 (2004).
5. Gurnis, M. & Hager, B. H. Controls on the structure of subducted slabs. *Nature* **335,** 317–321 (1988).
6. Christensen, U. R. The influence of trench migration on slab penetration into the lower mantle. *Earth Planet. Sci. Lett.* **140,** 27–39 (1996).
7. Zhong, S. & Gurnis, M. Interaction of weak faults and non-newtonian rheology produces plate tectonics in a 3D model of mantle flow. *Nature* **383,** 245–247 (1996).
8. Kincaid, C. & Olson, P. An experimental study of subduction and slab migration. *J. Geophys. Res.* **92,** 13832–13840 (1987).
9. Griffiths, R. W., Hackney, R. I. & van der Hilst, R. D. A laboratory investigation of effects of trench migration on the descent of subducted slabs. *Earth Planet. Sci. Lett.* **133,** 1–17 (1995).
10. Russo, R. M. & Silver, P. G. Trench-parallel flow beneath the Nazca Plate from seismic anisotropy. *Science* **263,** 1105–1111 (1994).
11. Wortel, M. J. R. & Spakman, W. Subduction and slab detachment in the Mediterranean-Carpathian region. *Science* **290,** 1910–1917 (2000).
12. Peyton, V. *et al.* Mantle flow at a slab edge; seismic anisotropy in the Kamchatka region. *Geophys. Res. Lett.* **28,** 379–382 (2001).
13. Turner, S. & Hawkesworth, C. Using geochemistry to map mantle flow beneath the Lau Basin. *Geology* **26,** 1019–1022 (1998).
14. Gvirtzman, Z. & Nur, A. The formation of Mount Etna as the consequence of slab rollback. *Nature* **401,** 782–785 (1999).
15. Pearce, J. A., Leat, P. T., Barker, P. F. & Millar, I. L. Geochemical tracing of Pacific-to-Atlantic upper mantle flow through the Drake passage. *Nature* **410,** 457–461 (2001).
16. Govers, R. & Wortel, M. J. R. Lithosphere tearing at STEP faults: Response to edges of subduction zones. *Earth Planet. Sci. Lett.* **236,** 505–523 (2005).
17. Schellart, W. P. Kinematics of subduction and subduction-induced flow in the upper mantle. *J. Geophys. Res.* **109,** B07401, doi:10.1029/2004JB002970 (2004).
18. Kincaid, C. & Griffiths, R. W. Laboratory models of the thermal evolution of the mantle during rollback subduction. *Nature* **425,** 58–62 (2003).
19. Dvorkin, J., Nur, A., Mavko, G. & Ben-Avraham, Z. Narrow subducting slabs and the origin of backarc basins. *Tectonophysics* **227,** 63–79 (1993).
20. Schellart, W. P., Lister, G. S. & Toy, V. G. A Late Cretaceous and Cenozoic reconstruction of the Southwest Pacific region: Tectonics controlled by subduction and slab rollback processes. *Earth-Sci. Rev.* **76,** 191–233 (2006).
21. Stegman, D. R., Freeman, J., Schellart, W. P., Moresi, L. & May, D. Influence of trench width on subduction hinge retreat rates in 3-D models of slab rollback. *Geochem. Geophys. Geosyst.* **7,** Q03012, doi:10.1029/2005GC001056 (2006).
22. Vogt, P. R. Subduction and aseismic ridges. *Nature* **241,** 189–191 (1973).
23. Kerr, R. C. & Lister, J. R. The effects of shape on crystal settling and on the rheology of magmas. *J. Geol.* **99,** 457–467 (1991).
24. Kley, J. & Monaldi, C. R. Tectonic shortening and crustal thickness in the Central Andes; how good is the correlation? *Geology* **26,** 723–726 (1998).
25. Coblentz, D. D. & Richardson, R. M. Analysis of the South American intraplate stress field. *J. Geophys. Res.* **101,** 8643–8657 (1996).
26. Ghosh, P., Garzione, C. N. & Eiler, J. M. Rapid uplift of the Altiplano revealed through ^{13}C-^{18}O bonds in paleosol carbonates. *Science* **311,** 511–515 (2006).
27. DeMets, C., Gordon, R. G., Argus, D. F. & Stein, S. Effect of recent revisions to the geomagnetic reversal time scale on estimates of current plate motions. *Geophys. Res. Lett.* **21,** 2191–2194 (1994).
28. O'Neill, C., Müller, D. & Steinberger, B. On the uncertainties in hot spot reconstructions and the significance of moving hot spot reference frames. *Geochem. Geophys. Geosyst.* **6,** Q04003, doi:10.1029/2004GC000784 (2005).
29. Barker, P. F. Scotia Sea regional tectonic evolution: implications for mantle flow and palaeocirculation. *Earth-Sci. Rev.* **55,** 1–39 (2001).
30. Sdrolias, M. & Müller, R. D. Controls on back-arc basin formation. *Geochem. Geophys. Geosyst.* **7,** Q04016, doi:10.1029/2005GC001090 (2006).

Supplementary Information is linked to the online version of the paper at www.nature.com/nature.

Acknowledgements We thank O. Oncken, R. Kerr, G. Davies and V. Toy for discussions on subduction processes, mantle dynamics, Andean geology and plate kinematics. We also thank R. Griffiths, M. Sandiford, B. Kennett and D. Müller for providing comments on an early version of the manuscript. Finally, we thank APAC, ACcESS, and VPAC for computational resources and staff from VPAC for technical assistance.

Author Information Reprints and permissions information is available at www.nature.com/reprints. The authors declare no competing financial interests. Correspondence and requests for materials should be addressed to W.P.S. (wouter.schellart@anu.edu.au).